Hindawi
Advances in Civil Engineering
Volume 2023, Article ID 4290824, 18 pages
https://doi.org/10.1155/2023/4290824

Research Article

Response Analysis of a Ballasted Rail Track Constructed on Soft Soil by 3D Modeling

Iram Lamiya Hoque,[1] **Shamontee Aziz**,[1] **Joya Rani Mallick**,[1] **Md. Arifuzzaman Nayeem**,[1] **Tamanna-E-Hafiz Maisha**,[1] **F. M. Zahid Hossain**,[2] **and A. F. M. S. Amin**[1]

[1]*BUET-JIDPUS, Bangladesh University of Engineering and Technology, BUET-JIDPUS Academic Building, Dhaka 1000, Bangladesh*
[2]*Army Headquarters, Dhaka 1206, Bangladesh*

Correspondence should be addressed to A. F. M. S. Amin; samin@ce.buet.ac.bd

Received 19 August 2022; Revised 29 December 2022; Accepted 6 January 2023; Published 4 February 2023

Academic Editor: Zhi Cheng Tang

The displacement, stress, and strain distributions of railway embankments on the soft deltaic deposit of the Ganges–Brahmaputra floodplain are investigated. A numerical model developed in general-purpose finite element software is used to simulate the design train load on a deltaic deposit for a 100 km/hr rail speed. The numerical analysis analogy is grounded in the spring model, where a beam under the unit load is modeled based on the Winkler foundation model concept. In the moving load simulation on soil, the static point load relating to the axle load is assigned in the form of a dynamic multiplier, determined using auxiliary software. The calculated shear force in terms of the influence line is applied as a dynamic multiplier. The numerical results demonstrate that under a dynamic train load, the loose ballast undergoes larger and more erratic displacement than the subballast. Comparative analysis between varying subballast stiffnesses shows that stiffer subballast yields smaller displacements. Moreover, a high subballast stiffness can counterbalance the potential of forming permanent deformation by generating lower strains. However, a stiffer subballast does not play a prominent role in reducing the displacement of ballast or vertical stresses. The subgrade is found to carry the maximum load, withstanding the maximum vertical stress; thus, the importance of using an improved subgrade with higher stiffness is also observed. A greater subgrade stiffness improves its load-carrying capacity but fails to reduce the tension responsible for the lateral spreading of the soft subsoil. To reduce the high radial strain, the effects of improving the stiffness properties of two immediately adjacent soft soil layers are numerically investigated. The improvement of subsoil alone is effective in reducing the radial strain, whereas the improvement of both subgrade and subsoil produces further reductions. The critical train speed generating the maximum displacement is identified as 120 km/hr, and the dynamic velocity amplitude decreases with depth. Finally, an allowable limit of rail embankment settlement on a soft deltaic deposit is observed.

1. Introduction

The floodplain of the Ganges–Brahmaputra delta needs to have new rail tracks to facilitate the development initiatives of Bangladesh, providing a gateway for international rail traffic and freight transportation [1, 2]. In British India, it was not techno-economically feasible to construct a railway track in the southern part of present-day Bangladesh due to the unique soft soil characteristics of the Ganges–Brahmaputra floodplain [3]. These characteristics include cyclic expansion and contraction due to wetting and drying, soil accumulation, and erosion in each flood season, which can prompt a large amount of settlement as well as differential settlement [4, 5]. Despite this challenging soil, it is of utmost importance to build railroads in this southern zone through the Padma Bridge Rail Link Project to provide the missing connectivity between Southeast Asia and the Trans-Asian (TA) rail track network. The opening of the Padma Bridge [6, 7] is the first attempt in this endeavor.

The train track structure is a compound structure with layers of ballast, subballast, subgrade, and subsoil (Figure 1) [8]. To understand the track behavior satisfactorily,

numerical simulations of train load on the rail track structure and subsequent analysis have been presented in the literature (i.e., [9–18]). The dynamic train load demands the selection of an appropriate material model for numerical analysis that can better apprehend the stress-strain behavior of embankments and subsoil. Previous studies have used linear elastic models [16, 19], Mohr–Coulomb models [14, 16, 20–25], hardening soil (HS) models [14, 26], modified Cam-Clay models [24], and hardening soil models with small strain stiffness (HS-small) [18]. Among these, the HS-small model can simulate soil stiffness at very small strains and its nonlinear dependency on strain amplitude [27], which is crucial to consider for predicting soil behavior under dynamic train loads. However, limited studies that consider this attribute of all the layers of track structure for analysis have been reported in the literature.

The transmission of a train load through the rail structure and the subsequent response of the individual track components are dependent on important elements, i.e., subballast, subgrade, and soil properties [28, 29]. The dynamic response of a rail track is also strongly associated with the material characteristics that define the stiffness of its constituents. As train-induced vibrations become more prominent, a larger settlement is expected in track structures with ballast or subballast made of low-stiffness materials [18, 30]. Subgrade has been responsible for many past cases of track failures, as little can be done to improve the subgrade during maintenance operations [29]. Moreover, when the track embankment is constructed on soft subsoil, the possibility of differential settlement and dynamic response amplification may lead to bearing capacity failure and potentially put the safety of the track at risk [24, 31] (see also Figure 1). Soil structure also affects lateral deformation [32]. Delayed lateral deformations can be significant for clay foundations [33], as 20% of the total settlements have been reported to be due to lateral deformations [34]. Most related studies observed the lateral deformations of road embankments [33, 35, 36] but did not examine the lateral deformation or strain distribution of the soft subsoil of railway embankments under dynamic train loads.

Due to the obvious constraints, the operation of train tracks over soft ground often requires imposing a critical speed or cutoff speed. A train running over the soft terrain at a speed higher than this critical speed causes large settlements on the track, and with time, track degradation results from cumulative plastic deformation and progressive failure. Consequently, this affects the overall riding quality as well as the efficiency of the transportation system. Thus, a stringent analysis of stress, strain, and settlement characteristics for safer train operation is needed. Although Poulos et al. [37] and Long et al. [38] have studied the behavior of rail tracks on marine soft clays, rail system performance on the alluvial deposits of the Ganges–Brahmaputra floodplain has not yet been reported. Additionally, there is an absence of integrated studies on how superstructure (ballast, subballast, and subgrade) properties affect the soft deltaic subsoil during operation.

To address the aforementioned scenarios, in the current study, a numerical investigation was performed (i) to idealize the settlement characteristics, stress, and strain responses of the newly constructed rail track structure over the Ganges–Brahmaputra basin with varying subballast and subgrade stiffness, (ii) to observe the comparative contribution of subgrade and subsoil improvement in reducing lateral strains, and (iii) to determine the critical speed for reviewing whether the material characteristics of the current track structure can allow the future speed demand. The present study is the first attempt to predict the behavior of rail tracks on such challenging alluvial deposits. The results provide insight into crucial parameters to be considered for the satisfactory performance and expansion of the rail network for future trade opportunities.

2. Methodology

2.1. Study Area. The selected study area is in the Ganges–Brahmaputra floodplain. A 162 km rail track, both ballasted and ballast-less, is being constructed on this soft deltaic deposit. The rail track and embankment system considered for this study are selected based on the underlying soil characteristics. As this study focuses on the behavior of soft deltaic deposits, a borehole containing layers of soft soil is selected by consulting the available soil test reports. The selected borehole (23°35′43.3″N, 90°18′41.7″E) encounters different soil layers, among which the first two are silt and clay with very low standard penetration test (SPT) values (SPT N: 2–5). Layer 1 contains sand with trace silt, and layer 2 is silt with clay. The next layers are silty fine sand (see also Figure 1), where the SPT value increases with increasing depth.

2.2. Numerical Modeling

2.2.1. Model Selection for the Rail Embankment System. The material model selected for the embankment and subsoil of this study is the HS-small model. This model was chosen because it works in the elastoplastic range. Moreover, the nonlinearity of soil corresponding to hardening laws and plastic flow rules are properly accounted for in this model. The rail is designed as a beam element. The properties of the rail are set according to the standard UIC 60 rail [16] that is used in the selected rail track of this study. The standard sleeper is modeled with solid sections with the properties of a prestressed concrete section [16]. The rail clip is modeled using the node-to-node anchor connected to the steel rail sections. The rail, sleeper [39], and rail clip are modeled using a linear elastic model.

Three subballast stiffnesses are considered for a 25-ton axle load, and the axle distribution is shown in Figure 2. The considered speed is 100 km/h, which is the maximum operational speed for the considered railway track in this study, that is, the Padma Bridge Rail Link.

2.2.2. Geometry and Material Characterization. The embankment consists of layers of ballast, subballast, prepared subgrade, and embankment fill, as shown in Figure 3. The ballast material is crushed stones, whereas the subballast

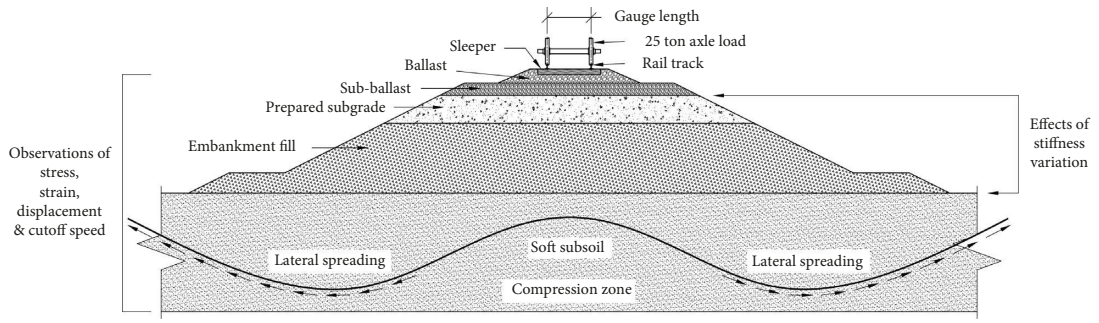

Figure 1: Schematic representation of the rail track system.

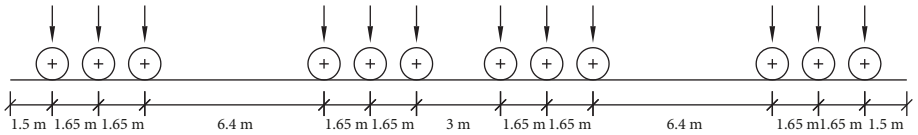

Figure 2: Position of the axles of the 25-ton locomotive (wheel-to-wheel distance in mm).

material is stone chips. The Los Angeles abrasion (LAA) (ASTM C 131) value of the subballast is less than 35%, and the minimum soaked California bearing ratio (CBR) (ASTM D1883-21) value is 25 when compacted at 100% of its modified Proctor density. The coefficient of uniformity is $C_u \geq 7$, and the coefficient of curvature C_c is between 1 and 3 from particle size analysis of soil (ASTM D422). The subgrade material is a mix of sand and brick chips at a ratio of 70 : 30.

For the numerical analysis, the material parameters, e.g., the saturated and unsaturated densities, Poisson's ratio, and shear modulus, are determined according to the characteristics of the soil of the selected embankment sections. Next, the advanced parameters (oedometric, tangent, unloading/reloading Young's modulus, and reference shear modulus) are set for the HS-small model. The parameters are determined according to the suggested values in the PLAXIS material model version 2021. The calculated properties are summarized in Table 1. Other parameters, including density, cohesion, and angle of friction, are based on the site-specific soil test report collected from the Padma Bridge Rail Link Project report [8].

The subballast was also modeled with the parameters used for the Tampere-Seinäjoki railway line in the study by Kalliainen et al. [40] for a comparative analysis of the effect of subballast materials on embankment behavior. Kalliainen et al. [40] obtained the stiffness parameters of two subballast materials, denoted as P90 Dense and P86 Dense, from cyclic triaxial tests. The parameters considered by both the present and previous studies are presented in Table 2.

2.3. Determination of the Natural Frequency and Shear Wave Velocity. To determine the dynamic properties of the subsoil, ambient vibrations at the selected embankment are recorded and analyzed using a microtremor device. The data are collected using a GEODAS15-HS data acquisition system [41]. Vibration measurements are carried out for 30–45 minutes with a sampling frequency of 100 Hz. The recorded ambient data are processed using Easy HVSR software following the technique of Nakamura [42, 43], and the natural frequency of in situ vibration, the shear wave velocity profile with depth, and the average shear wave velocity up to 30 m depth (V_{s30}) are determined.

The recorded microtremor data are imported into the software and divided into window frames using an in-built automatic window selection option with a temporal dimension of at least 20 seconds, as recommended by the Site Effects Assessment using Ambient Excitations (SESAME) project [44]. For H/V spectral analysis, these windows are then filtered with a passband of 0.5–15 Hz to discard any source of interference affecting the analysis, and a subsequent Fourier transformation is performed to obtain the average spectra. To eliminate high-frequency oscillations, the Fourier transforms are also smoothed using the smoothing technique "Triangular Proportional" with 10% smoothing and 5% tapering. The natural frequency of in situ soil is then obtained from the frequency value corresponding to the peak of the average H/V spectral ratio. A reliability check of the H/V average curve and its peak is also performed according to the conditions referred to by the SESAME project. The standard deviation of the natural frequency value was kept within ±0.5 Hz. Figure 4 shows the average H/V spectral ratio and its confidence interval as a function of frequency at the embankment location.

Figure 5 shows the shear wave velocity profile along with its depth at the selected embankment section. For this, the shear wave velocity of the first layer was estimated using an empirical correlation between the V_s and N values, as stated in Rahman et al. [45]. The shear wave velocity of the following layers was iterated while keeping the soil layer thickness, unit weight, and Poisson's ratio constant [46]. The obtained result of V_s was used to verify the natural frequency obtained from the field data using the following equations [47–49]:

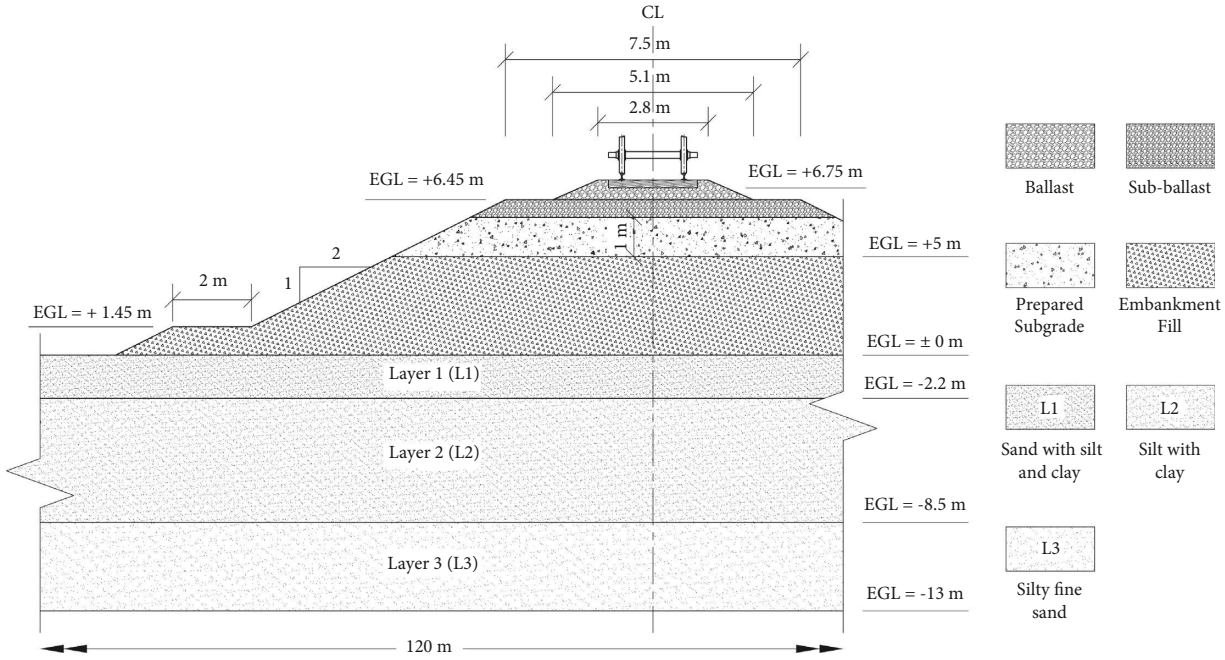

Figure 3: Schematic diagram of the embankment and subsoil.

Table 1: Material properties for the different layers of embankment and subsoil.

Material model	Unit	Ballast HS small	Subballast HS small	Prepared subgrade HS small	Embankment fill HS small	Layer 1 HS small	Layer 2 HS small	Layer 3 HS small	Layer 4 HS small
Drainage type		Drained	Drained	Drained	Drained	Drained	Drained	Drained	Drained
γ_{unsat}	kN/m^3	16	20	20	19.7	15	17	17	18
γ_{sat}	kN/m^3	18	23	21.8	21.8	17	19	19	20
e_{init}		0.74	0.52	0.52	0.52	0.66	0.77	0.66	0.66
c'_{ref}	kPa	0	0	0	0	25	48	0	0
φ'	Deg	50	55	60	38	30.7	28.9	38.7	40.7
G_{0ref}	kN/m^2	50000	130300	130300	90000	70000	33300	112500	112500
ν_{ur}'		0.2	0.2	0.2	0.3	0.15	0.2	0.2	0.2

Table 2: Input parameters for the subballast and subgrade materials.

	Present study	P90 dense	P86 dense
		Kalliainen et al. [40]	
	Subballast		
Drainage	Drained	Drained	Drained
E_{50}^{ref} (kPa)	28850	31250	50000
E_{oed}^{ref} (kPa)	28850	31250	50000
E_{ur}^{ref} (kPa)	86500	140000	125000
	Subgrade		
Drainage	Drained	Drained	Drained
E_{50}^{ref} (kPa)	60000	60000	60000
E_{oed}^{ref} (kPa)	45000	45000	45000
E_{ur}^{ref} (kPa)	180000	180000	180000

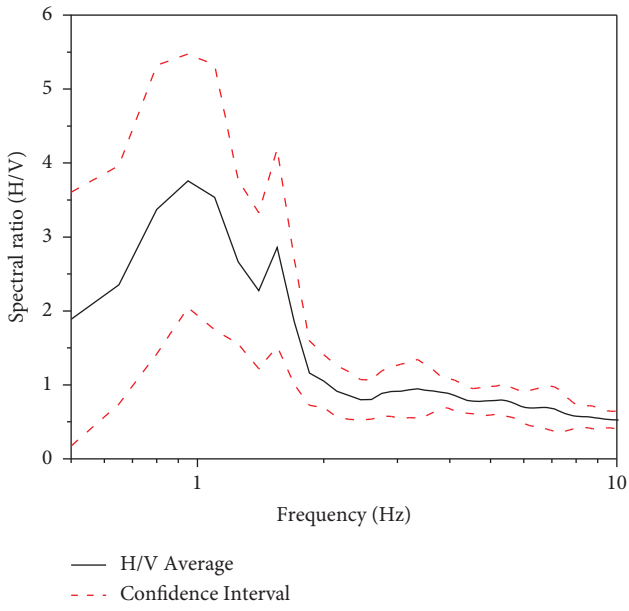

Figure 4: H/V spectral ratio as a function of frequency.

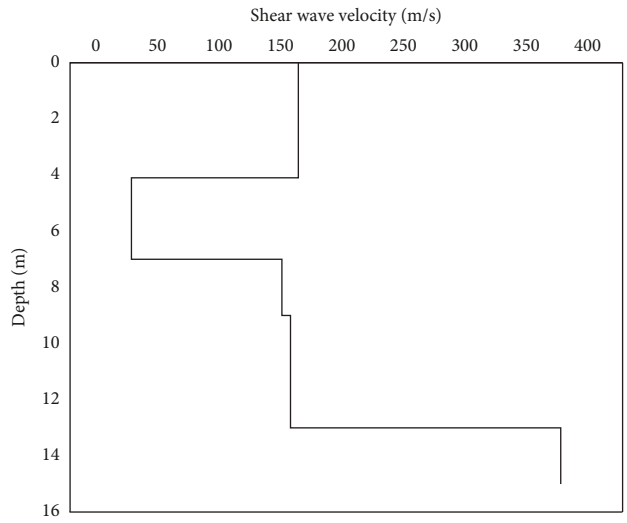

Figure 5: Shear wave velocity profile.

$$s = \sqrt{\frac{(1-2\mu)}{2(1-\mu)}}, \tag{1}$$

$$f_n = \frac{V_s}{2\pi sh} = \sqrt{\frac{G}{\rho}}\ \frac{1}{2\pi sh}. \tag{2}$$

Here, V_s is the shear wave velocity of the soil layer, h is the thickness of the soil layer, and s is a coefficient that is determined from Poisson's ratio of the soil.

2.4. Determination of Damping Coefficients and Critical Frequency. To demonstrate the actual damping effect of the wave propagation from train movement, material damping characterizations are introduced to decrease the velocity in the deeper layers. Target frequencies (lowest = 0.5 Hz and highest = 1.02 Hz) and natural angular frequency are given as input parameters for determining the damping coefficients (Rayleigh coefficients α, β). The target frequencies are chosen to search for the critical frequency for the given damping ratio ($\xi = 0.2\%$ for soft soil). The natural angular frequency of the soil layers in both directions can be expressed by the following equation, where V_s is determined from the microtremor analysis:

$$\omega_{nz} = \frac{V_s}{sh}\sqrt{\frac{(1-2\mu)}{2(1-\mu)}}. \tag{3}$$

2.5. Boundary Condition and Mesh Size. The length, width, and height of the model are 120 m (X-axis), 60 m (Y axis), and 6.6 m (Z axis), respectively. The three-dimensional finite element method (FEM) was used in this study for numerical modeling and analysis using PLAXIS software. The deformation boundary condition is set to default under the model condition. In the case of dynamic analysis, considering the moving wheels, the generated waves might reverberate from the boundaries, so the boundaries are set to be viscous boundaries. The generated mesh is very fine, with a coarseness factor of 0.05 in embankment sections, to properly accommodate the effect of the stiffness of the ballast and subballast near the wheel locations. Away from the embankment, a finer mesh is used, as shown in Figure 6(a), to complete the analysis in less time.

2.6. Phase Construction. The numerical computations are completed in seven phases. The first six phases are the construction stage in which the subsoil and embankment sections are constructed, generating the initial stresses. To achieve the effect of consolidation, the drainage condition is selected as drained. At the end of phase six, the rail, sleepers, and rail clips are activated. Following phase six, phase seven is calculated to simulate the dynamic train load on the whole embankment system, as shown in Figures 6(b)-6(c).

2.7. Dynamic Load Determination. To simulate a train load, static analysis to produce the shear force distribution of a beam resting on an elastic medium is carried out using three-dimensional building information modeling (BIM) by PROKON (structural engineering software). This approach uses the spring concept of a beam constructed on a Winkler foundation [50–55], and it is applied for defining the soil and rail track systems. In this procedure, the rail track and sleepers are modeled as beam elements and elastic spring elements, respectively. The shear force throughout the beam is recorded for every 0.6 m movement of the train wheel in the forward (Y) direction. In the subsequent steps, these data are processed to calculate the influence line in every sleeper position along the track. Dividing the wheel position by the train velocity, the shear force with respect to time for each sleeper is generated, and the dynamic multiplier properties are determined. Then, data are incorporated into PLAXIS

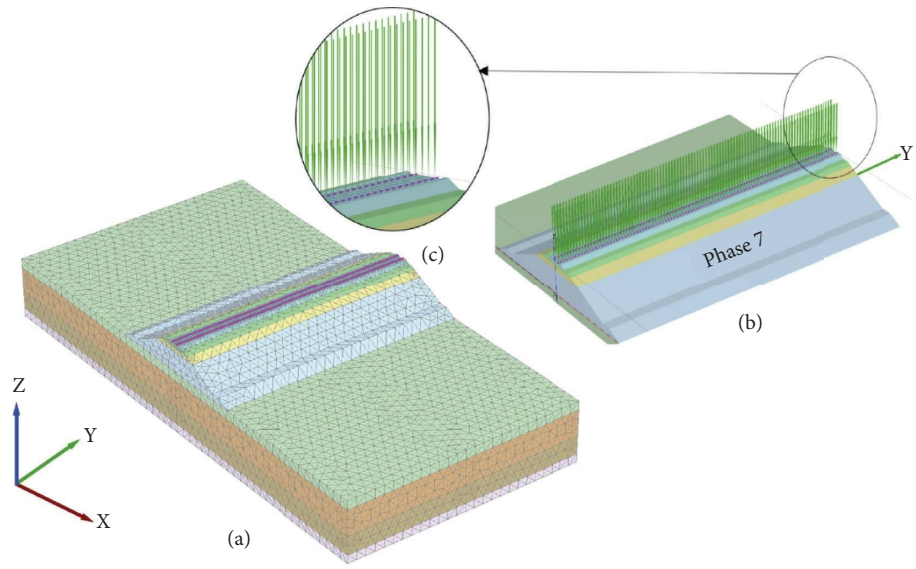

Figure 6: FEM model: (a) meshed model; (b-c) activation of train load in phase 7.

through its built-in dynamic load multiplier attribute, as shown in Table 3. Earlier, Shahraki et al. [16] studied the effect of train loads on organic and peat soils by using dynamic multipliers in PLAXIS. As this is a complex model combining a significant number of components (train, rail, sleeper, clip, dynamic load, embankment, and subsoil), a script is developed to systematically generate multiple dynamic models in a time-efficient manner.

3. Results and Discussion

3.1. Displacement of Ballast and Subballast for Different Subballast Stiffnesses. A plot of vertical displacement along the longitudinal axis is delineated in Figures 7(a)–7(f) just before the first train axle leaves the rail track for all three subballast cases. These figures also show the comparative behavior between the ballast layer and subballast layer, where the latter has different stiffnesses in the order of soft deltaic deposit < P90 Dense < P86 Dense.

Figures 7(a)–7(c) show that the maximum displacement of the ballast is 0.07 m for all three subballast cases. For the subballast of the present study, the maximum displacement is close to 0.012 m, as seen in Figure 7(d). Thus, the ballast exhibits a settlement almost 6 times greater than that of the subballast, as the former is the nearest point of contact from the wheels. This signifies that away from the wheel, the amplitude of the vertical displacement decreases. Moreover, the ballast is displaced in both the upward and downward directions, showing a fluctuating displacement. Ballast, being the first layer, absorbs shocks from the dynamic train load [56], and the response is a typical response of displacement under dynamic loading. The train wheel load can be considered a repetitive impact (small duration impulse load) loading, which together with the "denseness" of ballast (stone dominant) offers a low level of damping in the responses causing the fluctuation seen in Figures 7(a)–7(c). Subballast consists of particles smaller than those of the ballast. The energy dissipated by sliding friction is higher in smaller particles, which also exhibit a higher number of contacts [57]. This will result in better damping, and thus, a more consistent pattern of displacement is noticed for the subballast where the displacement is smaller than the ballast.

As already mentioned, the ballast displacement is the same for all three considered subballast stiffnesses. Hence, the stiffness of the subballast does not affect the ballast displacement. In contrast, the lower stiffness properties of the subballast of the soft deltaic deposit result in slightly more displacement than in the P90 dense and P86 dense cases, as seen in Figures 7(d)–7(f).

Figure 7(g) presents how the displacement changes along with the depth of the embankment for subballast of different stiffnesses. As the depth increases, the displacement decreases. The soft deposit of this study deforms 1.3%–2% more than the P86 dense and P90 dense subballasts, at a depth of +5 m from the existing ground level (EGL).

However, at the bottom of the soil layer, e.g., at a depth of 15 m, the deltaic deposit deforms by more than 9% and 4% compared to the P86 dense and P90 dense, respectively. Thus, the data from the soft deposit always plot to the left of the other two materials of higher stiffness having higher displacement.

3.2. Effect of Subballast Stiffness on Shear Strain. Figure 8 presents the plots of shear strain at different depths. Here, with decreasing stiffness (i.e., P86 dense > P90 dense > - present study), the shear strain increases slightly. The strain associated with soft deltaic deposits rises by 9% compared to that associated with the P86 dense subballast. This shows that a larger shear strain occurs in a softer material. The shear strain is in the range of 10^{-4} for the subballast, and for the subgrade, the range is 10^{-4} to 10^{-3}. This strain range can simulate permanent deformation [58]. However, in the soil layers, the shear strains decay to 10^{-5}, which is less than 10^{-4},

Table 3: Dynamic multipliers for the train load analysis.

Time steps	Distance	Time	Multiplier 1	Multiplier 2	...	...	Multiplier 99	Multiplier 100	Multiplier 101
1	0	0.00	0	0	...	...	0	0	0
2	0.6	0.03	0	0	...	...	0	0	0
3	1.2	0.06	0	0	...	...	0	0	0
4	1.8	0.09	0	0	...	...	0	0	0
5	2.4	0.12	0.069	−0.031	...	...	0	0	0
6	3	0.15	−0.07	0.078	...	...	0	0	0
...	...	...	...	...	...	...	...	...	...
...	...	...	...	...	...	...	...	...	...
98	58.2	2.99	0	0	...	...	0	0	0
99	58.8	3.02	0	0	...	...	0	0	0
100	59.4	3.05	0	0	...	...	−0.01	0	0
101	60	3.09	0	0	...	...	0.05	−0.01	0

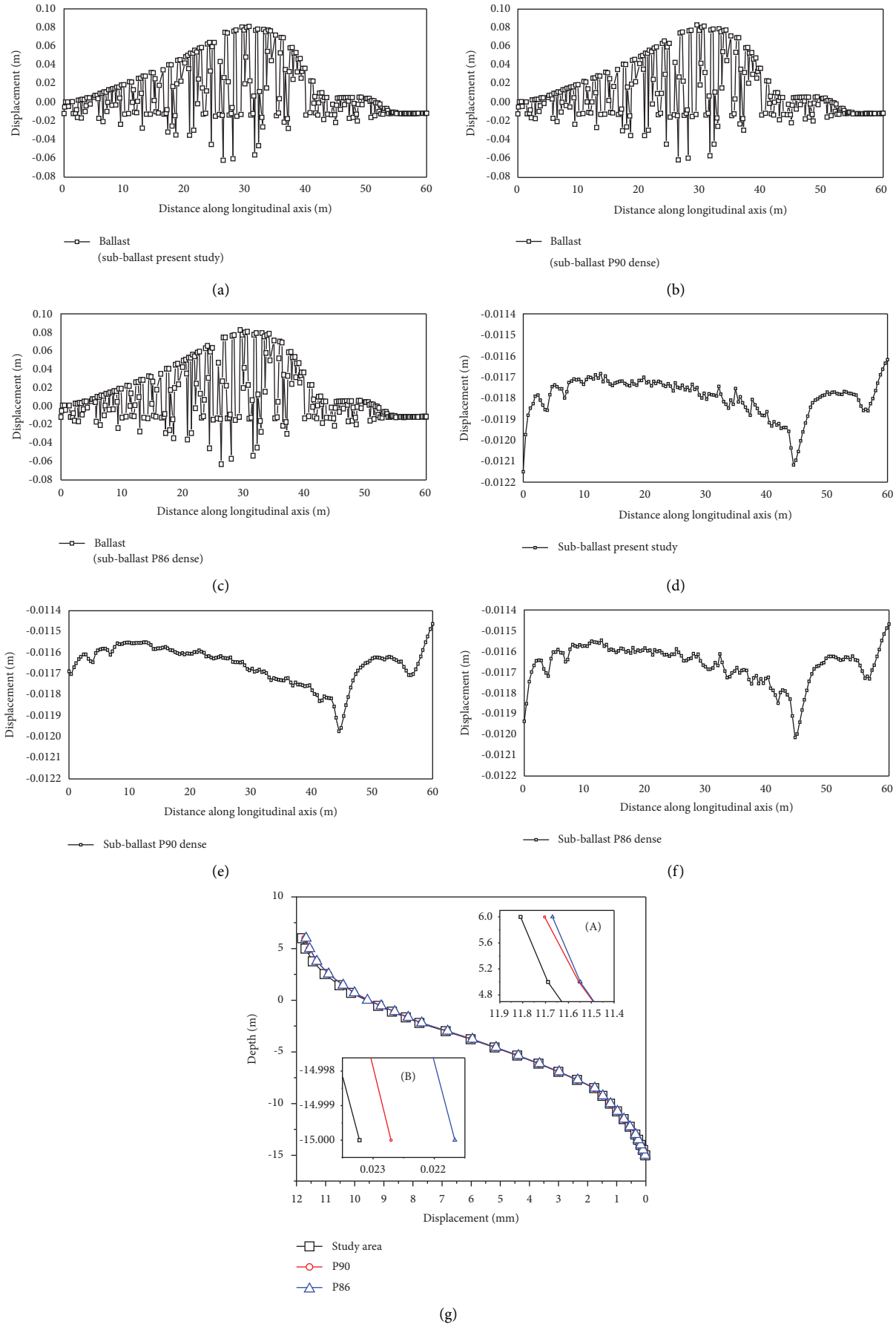

FIGURE 7: (a–c) Displacement vs. distance along the longitudinal axis for the ballast; (d–f) displacement vs. distance along the longitudinal axis for the subballast; (g) depth of embankment vs. displacement for varying subballast stiffnesses.

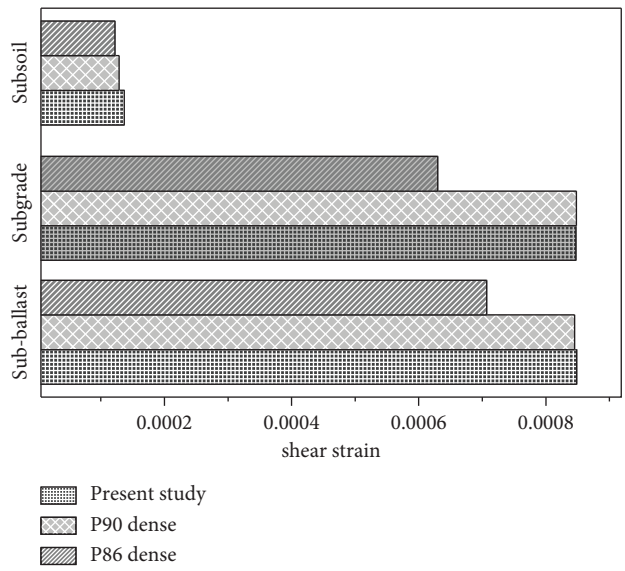

Figure 8: Shear strain at different depths for the subballast with different stiffnesses.

and the chances of permanent deformation in the soil are unlikely to occur under this study condition.

The generation of a larger strain occurs when loose material is used in a subballast, as confirmed by Kalliainen and Kolisoja [59]. Vinter and Tanttu [18] also stated that the use of loose subballast material increases the shear strain, resulting in permanent deformation. He also stated that the stiffness of subsoil is the most dominant factor for the accumulation of a larger strain. In this study, the stiffness of the first two subsoil layers is within 15–20 MPa, whereas Vinter and Tanttu [18] studied subsoil with a stiffness in the range of 10–200 MPa. From these results, it is observed that in the subballast layer (P90 Dense), the shear strain is 0.085% for the present study (sub-soil stiffness = 20 MPa), whereas in Vinter and Tanttu [18]; for the same subballast, the shear strain is 0.1% for a subsoil stiffness of 10 MPa. Hence, for similar subsoil stiffnesses, the obtained shear strains are close, which validates the numerical model of the present study. Again, in the present study, a loose subballast is used, and the shear strain in the loose subballast is 8.5% greater than that in the P86 dense subballast.

Thus, stiffness is the main controlling factor of the change in shear strain. This finding asserts that the use of loose material with low stiffness in subballast increases the vulnerability of developing larger plastic strains. Such loose subballast on top of soft subsoil may cause larger deformation, leading to the sinking of the ballasted track.

3.3. Effect of Subballast Stiffness on Vertical Stress. Figures 9(a)–9(c) show the vertical stresses along the longitudinal axis of the model with different stiffnesses of the subballast layer. All the stress points in Figure 9 are taken along the midsections of consecutive layers (i.e., ballast, subballast, and subgrade). These figures show that the effect of subballast stiffness is somewhat insignificant on the generated vertical stresses at different layers of the embankment. The tangent stiffness (E_{50}) of the subballasts of the present study, P90 dense case, and P86 dense case vary in a small range of 28850–50000 kPa. Thus, only a 13% difference in the vertical stress of the subballast is observed between the present study and the P86 Dense case, with the latter being greater.

However, one important observation is that the stresses in the subgrade are much higher than those in the ballast and subballast layers. The thickness of different layers of the railway track is an important factor that affects the vertical stress distribution [60]. Thus, a subgrade with a thickness greater than those of the ballast and subballast has a variation in stress that is different than those of the other two layers. The subgrade carries 240% more force per unit area than the subballast in the present study. The subgrades for the other two cases also show a similar increase in force per unit area compared to their respective subballasts. This signifies that the subgrade carries greater loads than the ballast or subballast when subjected to wheel loads [61] also showed that subgrade reactions to wheel loads are larger than subballast and ballast reactions.

3.4. Effect of Subgrade Stiffness on Vertical Stress. Figure 10 summarizes the variation in vertical stress in response to the different stiffnesses of the subgrade materials investigated. In Figure 9, the tangent stiffness of the subgrade is $E_{50} = 60$ MPa, whereas, in Figure 10, cases with 100 MPa and 200 MPa are also depicted. These results indicate that as the stiffness increases to 100 MPa, the maximum vertical stress increases by 24% compared to that for $E_{50} = 60$ MPa. The maximum force per unit area, e.g., stress, increases further as E_{50} increases to 200 MPa, and an increase of 50% is observed compared to the result for $E_{50} = 60$ MPa. Thus, stiffer subgrades are required to carry greater loads.

The magnitude of the vertical stress caused by the track on the subgrade is low. Abebe and Qiu [62] found that the

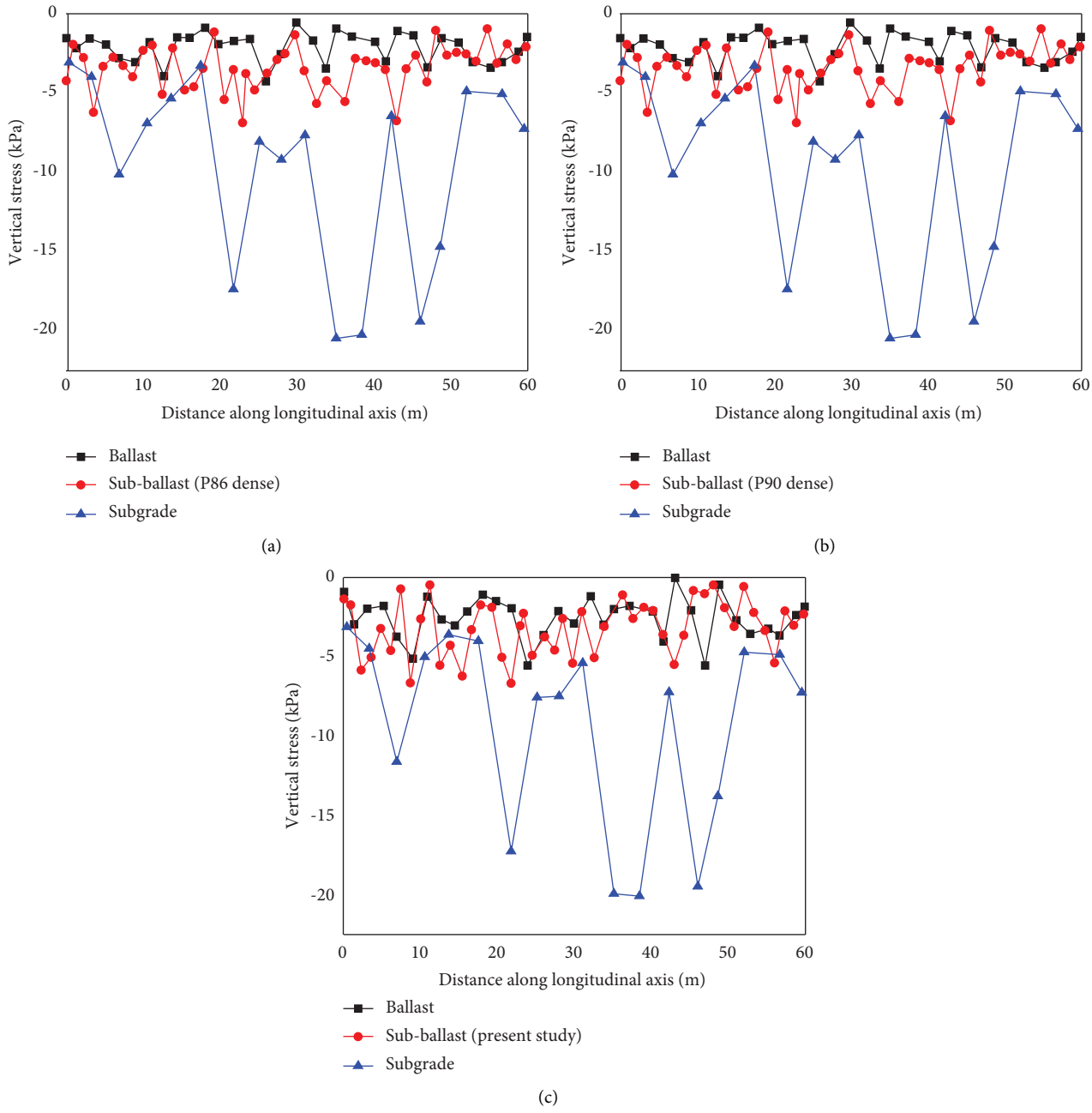

FIGURE 9: Vertical stress distribution along the longitudinal axis of the track: (a) P86 dense subballast material; (b) P90 dense subballast material; (c) present study.

maximum vertical stress caused by a high-speed train (350 km/hr) with an improved subgrade by introducing geogrids is 122 kPa. However, in this study, the speed is limited only to 100 km/hr with increased subballast and subgrade stiffness (60, 100, and 200 MPa). The average maximum vertical stress for the 200 MPa subgrade is 33 kPa for a 100 km/hr rail speed. However, increasing the load cycle with time may increase the stress because, with time, the particle interlocking of the ballast will increase, and it will transmit more load to the subgrade [63].

3.5. Effects of Subgrade Stiffness and Subsoil Improvement on Radial Strain. Figure 11 shows the distribution of the radial strain in the soil layers beneath the embankment fill. L_1 denotes the subsoil layer immediately under the embankment fill, while L_2 and L_3 are the consecutive layers. The strain measurements are taken along the midsection of each layer. Figure 11(a) represents the radial strain in the three subsoil layers with a subgrade with $E_{50} = 60$ MPa for deltaic deposits. L_2 shows the maximum radial strain, whereas L_3 shows the minimum radial strain. L_2, which contains soft

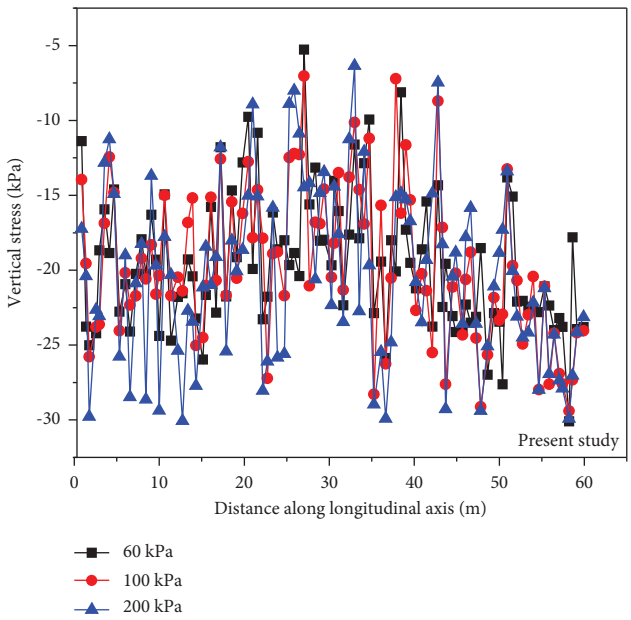

FIGURE 10: Changes in vertical stress along the longitudinal axis of the track for subgrades with different stiffnesses.

clay and silt, extends (i.e., a positive sign denotes compression, and a negative sign denotes tension) 75% more than L_3, which contains mostly sand. Compared to that in L_1, the radial strain is slightly higher in L_2, owing to the presence of a higher percentage of clay (15%) and silt (77%). Moreover, Figure 11 is a graphical representation of the compression and extension of the soil being subjected to a dynamic load. As an effect of the wheel load, plain strain is generated between the soil particles, followed by an arching effect between the gauges. The expansion generated by the particles of this zone is nullified by the expansion of the particles on the opposite side. As a result, this zone remains in compression throughout. On the other hand, particles outside of this zone expand laterally due to the absence of confinement in the soft soil. Figures 11(b) and 11(c) are graphical representations of radial strain in the subsoil of L_1 and L_2 with increasing subgrade stiffness. The properties of the subgrade are listed in Table 4. As the stiffness of the subgrade is increased from 60 MPa to 200 MPa, the radial strains in layers 1 and 2 remain unchanged.

Figures 12(a) and 12(b) represent the radial strains in the first two layers of soil, and the stiffnesses of both layers are improved. The stiffness of layer 1 is increased from 20 MPa to 35 MPa, whereas for layer 2, it is increased from 15 MPa to 30 MPa. Almost 33% and 58% reductions in radial strain are observed for L_1 and L_2, respectively, compared to the unimproved subsoil condition. The tension is reduced by 50% and 62.5% for L_1 and L_2, respectively, as both the subgrade and subsoil are further improved. Thus, from Figures 11 and 12, it can be inferred that for the soft deltaic deposit, an improvement in subgrade stiffness alone cannot reduce the radial strain. To reduce the radial strain in this type of soil, the improvement of the subsoil is necessary.

Figures 13(a)–13(d) show the color contours of the radial strain results without and with an improvement of the subgrade and subsoil stiffness. The outcome of Figure 13(a) can be explained as follows: contours inside the embankment but below the rail track show.

A circular zone of compressed soil (yellowish to red colored circular grids). Inside this grid, the presence of green-to-blue contours indicates the presence of soil undergoing expansion; similarly, dark-colored contours outside the rail track are dominant, indicating that a significant soil zone undergoes expansion, initiating lateral spreading of the soil. However, the expectation of geotechnical engineering in this regard would be that the soil throughout the influence zone of the embankment for the rail track will be under compression so that the lateral spreading tendency of soil is no longer effective or posing a threat to the instability of the whole track system.

Due to the high compressibility and low permeability of soft soil with a considerable amount of clay, the settlement process takes a long time to complete (consolidation settlement), and its magnitude accumulates with time; hence, the soil mass will remain in unstable conditions until the pore water pressure dissipates completely. In addition, a less stiff subgrade develops a larger radial strain, moving the underlying soft soil outward from the track and resulting in a large settlement. Less stiff subgrade spreads laterally, whereas stiffer subgrade resists spreading by developing lateral tensile strain [64]. Lateral spreading and settlement could accelerate in the absence of confinement if any water body or free space exists beside the embankment, which is likely for the considered case of deltaic deposits in this study. Because of the large settlements in the soft soil of the embankment, differential settlement within the embankment-viaduct-bridge system is unavoidable. This substantial differential settlement can create irrecoverable damage to the track and thus should not be allowed. To mitigate this issue, proper subsoil improvement methods along with denser and stiffer subgrade materials should be chosen. However, the economic viability and availability of such materials should be studied further.

3.6. Variation in Dynamic Velocity with Depth. The amplitude of the dynamic velocity decreases with increasing depth, which can be noted in Figure 14. This decay with each layer of embankment and subsoil is because of the decay of the wave owing to the material's damping. A major decrease in velocity is observed until the depth of the subgrade, which is also reported by Shahraki et al. [16]. It is also observed that initially until the dynamic time is 1.28 s, the velocity is quite low. After that, the velocity increases and fluctuates up to 2.13 s. Then, the velocity remains lower than previously observed until the train passes the whole stretch of the track at 2.16 s.

3.7. Determination of Critical/Cutoff Speed. Figure 15 shows the relationship between vertical displacement and train speed for different layers of the embankment and subsoil. At a speed of 120 km/h, the displacement near the track

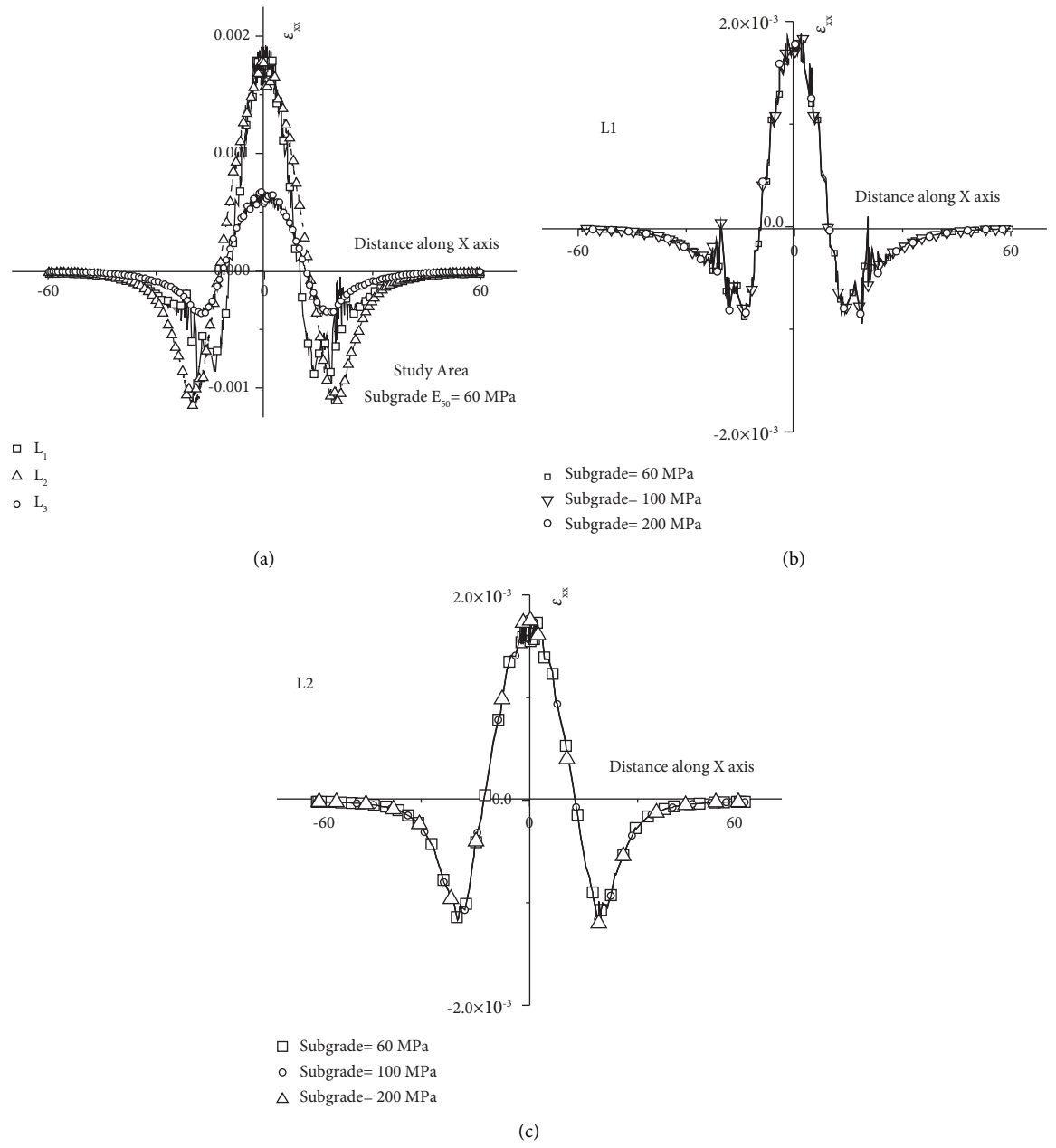

Figure 11: (a) Radial strain along the cross-section of the model for the deltaic deposit (subgrade E_{50} = 60 MPa); (b) variation in radial strain for varying subgrade stiffness (E_{50} = 60, 100, 200 MPa) for layer 1; (c) variation in radial strain for varying subgrade stiffness (E_{50} = 60, 100, 200 MPa) for layer 2 (see also Figure 3 and Table 4).

Table 4: Properties of the subgrade and subsoil are considered in Figures 11(a)–11(c) and 12(a)-12(b).

Variable	Reference figure	Stiffness values (E_{50}) Mpa			Case
		Subgrade (MPa)	L_1 (MPa)	L_2 (MPa)	
Subgrade stiffness	11(a)	60	20	15	—
	11(b) and 11(c)	60			
		100			
		200			
Subsoil stiffness	12(a) and 12(b)	60	20	15	I
			35	30	II

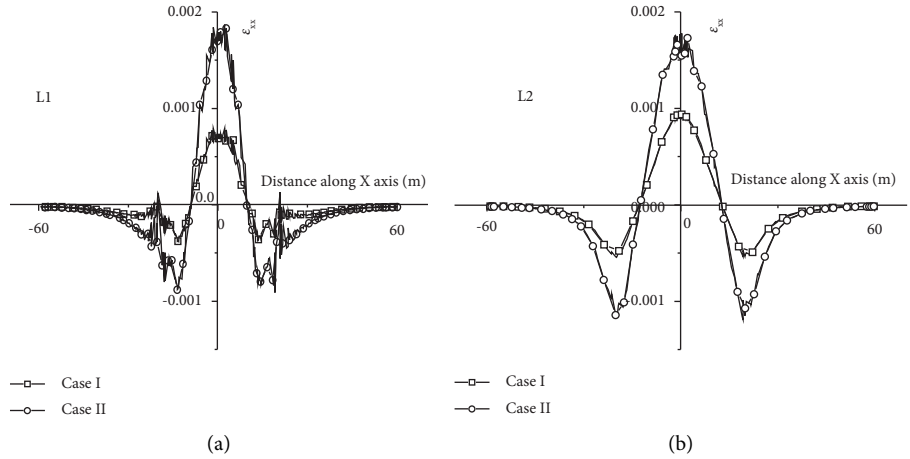

Figure 12: Radial strain along the cross-section of the model after soil improvement: (a) layer 1; (b) layer 2 (see also Figure 3 and Table 4).

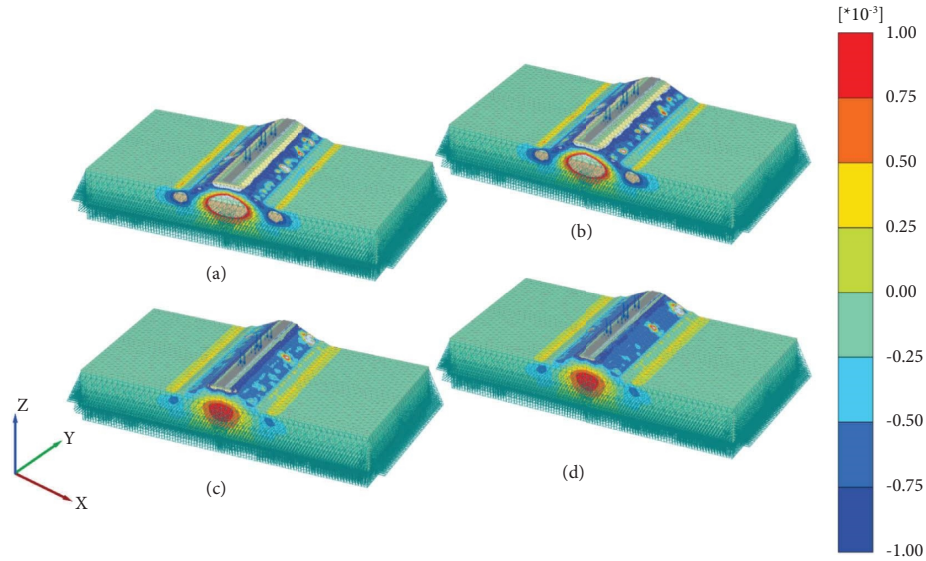

Figure 13: Color contours of the radial strain (a) without improvement of the subgrade or subsoil; (b) with the improvement of only the subgrade (E_{50} subgrade = 100 MPa for the deltaic deposit); (c) with the improvement of only the subsoil ($E_{50}L_1$ = 35 MPa, $E_{50}L_2$ = 30 MPa; E_{50} subgrade = 60 MPa); (d) with the improvement of both the subsoil and subgrade ($E_{50}L_1$ = 35 MPa, $E_{50}L_2$ = 30 MPa; E_{50} subgrade = 100 MPa).

surface is larger than those induced by all other considered speeds. According to Costa et al. [31] and Hu et al. [65]; the critical speed is the speed at which the maximum displacement of the track ground system is observed. For this study, the maximum amplitude for displacement was observed at 120 km/h. Hence, 120 km/h is the critical speed for this study. Speed ranges lower (70–100 km/h) and higher (125–200 km/h) than this are stated as subcritical and supercritical speed zones, respectively. The determination of the critical speed is required because it is important in the context of the differential settlement of the underlying soft soil [65]. When a train is moving, the propagated waves pass slowly through the soft soil, and the soil properties, e.g., density and water table, respond to the wave propagation. When the frequency of the train waves interacts with the natural frequency of the soil, a large amplification occurs, which sometimes deforms the track and the embankment structure permanently. This permanent deformation may lead to differential settlement of the track–soil system, which is undesirable for embankment-viaduct-bridge systems. Hence, to avoid this, it is desirable to run the train at a speed less than the critical speed, e.g., 120 km/h for the soft soil considered.

The displacement increases very slowly at both sub and supercritical speeds, whereas at 120 km/h, it increases sharply, as shown in Figure 16. At subcritical and supercritical speeds, the vertical displacement is somewhat constant, except at the cutoff speed. To reach any speed higher than 120 km/h, the train will cross this critical speed, and the maximum deformation will occur. Hence, it is

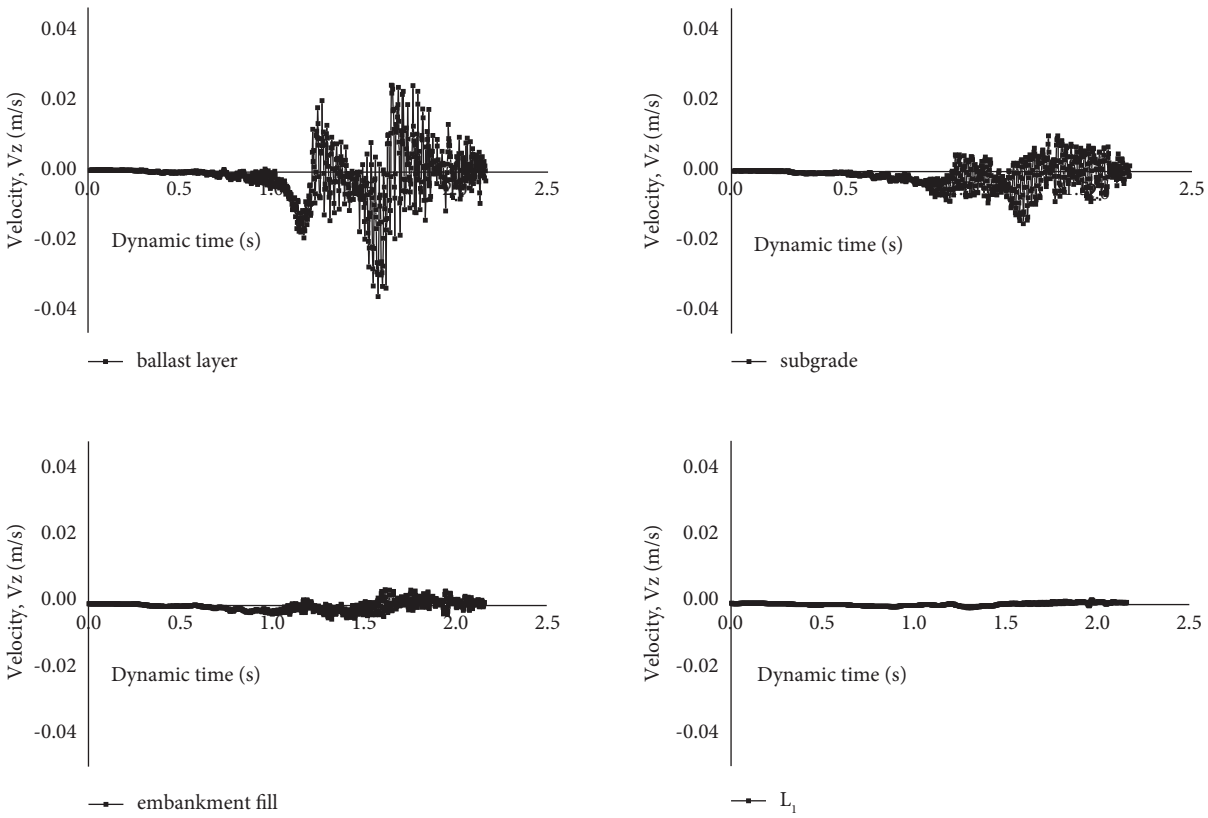

Figure 14: Vertical velocity vs. dynamic time profile at different layers of the rail track.

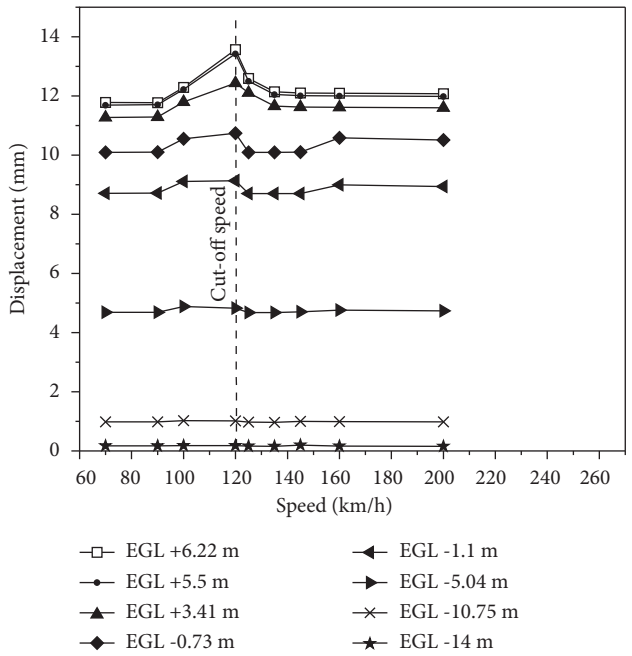

Figure 15: Displacements of different layers for varying train speeds.

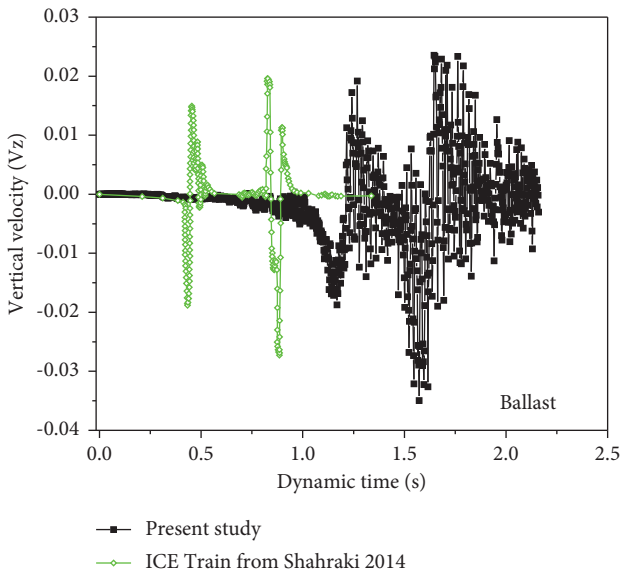

Figure 16: Vertical velocity vs. dynamic time for the present study and from Shahraki et al. [16].

always desirable to keep the speed of the train less than 120 km/h for the 25-ton axle load studied here. The design report of the Padma Bridge Rail Link, which was constructed on the soft deltaic deposit of the Ganges–Brahmaputra floodplain, also corroborates this observation [8]. The report also recommends a design train speed of less than 120 km/h: in particular, 100 km/h for an axle load of 25 tons.

Figure 16 also shows that the point nearest to a wheel generates the maximum displacement of 14 mm, whereas, at the point nearest to the EGL (−0.73 m from the EGL; a point in the embankment fill), the displacement is reduced by 24% compared to the former. A previous study by Jeon [66] recommends an allowable settlement of 10 mm for ballasted tracks. For speeds lower than that, Aziz et al. [67] recommended the allowable limit to be 15 mm. The maximum displacement for this study is thus within the allowable range. However, further verification is required from settlement sensors located in the field.

3.8. Comparative Analysis of the Present Model with the Model of Shahraki et al. [16]. The present model was compared with the study of Shahraki et al. [16]. Shahraki et al. [16] followed the same methodology for the incorporation of train load in PLAXIS by using dynamic multipliers. Their study investigated the behavior of peat and organic soil under an InterCity Express (ICE) train load. Figure 16 shows the change in the vertical velocity of the ballast over dynamic time for both studies. In both cases, the first peak in velocity is observed after the wheels cross the midspan of the rail track. This largely validates the present results in narrating the general behavior in local and global scenarios of the idealized problem in this paper. However, the time when the maximum velocity occurs is later in the present study. The potential reason behind this shift can be the lower speed of the present train, e.g., 100 km/hr, compared to the 180 km/hr of Shahraki et al. [16]; for which the train takes longer to cross the midspan. In the case of Shahraki et al. [16]; the third peak occurs in the positive direction, whereas for the present study, it occurs in the negative direction. As the train moves over the track, periodic waves are generated, which are affected by the characteristics of the train and sleeper spacing [16]. Although the sleeper configuration of both studies is the same, an ICE train has only four wheels, whereas the train adopted in the present study has thirteen wheels, which may have caused the variation in the patterns of vertical velocity. Further parametric studies will be required by changing the configuration of wheels and the speed to isolate their effects on dynamic velocity.

4. Conclusion

A numerical study is conducted as the first attempt to study the behavior of railway embankments constructed on the soft subsoil of the Ganges–Brahmaputra floodplain. A dynamic train load is simulated, and the effects of variations in the properties of the subballast, subgrade, and subsoil are investigated. The major observations from the study are as follows:

(1) Displacement patterns of ballast and subballast are estimated. Comparing their displacements, the former shows greater displacement owing to the proximity of the train wheels and the properties of the materials. Even after improving the stiffness of the subballast, the ballast displacements remain unchanged, and its effect on the subballast displacement is negligible. Looser and less stiff subballast exhibits larger shear strains (0.085% for subballast in this study). This, followed by soft deltaic subsoil may result in greater permanent settlements.

(2) An increased subballast stiffness does not influence the vertical stress of the ballast, subballast, or subgrade. However, the subgrade withstands the maximum vertical stress, and the higher the subgrade stiffness is, the greater the vertical stress. This increased stiffness reduces the chances of lateral spreading.

(3) Subsoil layers containing clay and silt exhibit radial strains larger than (75%) of those in sandy layers. It is inferred that increasing the subgrade stiffness alone cannot properly constrain the radial strain. The stiffness of the subsoil layers of soft deltaic deposits must be improved to reduce the radial strain and the probability of lateral spreading. This study shows that the slight improvement in stiffness in both the subgrade and soft subsoil layers decreases the lateral expansion between 33% and 58%.

(4) The results show that the dynamic velocity decreases with depth. However, at 120 km/hr, the displacements are the maximum observed for all the considered layers. Hence, 120 km/hr is considered the cutoff velocity for the studied railway track configuration.

(5) This study finds the maximum settlement (14 mm nearest to the wheel) to be within allowable limits, as determined by existing studies. Nevertheless, the current study recommends further investigation focusing on the validation of numerical results with field observations, as there remain no specific guidelines for the allowable settlement or influence of material properties on the operation of railways on soft deltaic deposits. However, researchers have to wait until this track goes into operation to collect the field data.

Data Availability

The data used to support the findings of this study are available from the corresponding author upon reasonable request.

Conflicts of Interest

The authors declare that they have no conflicts of interest.

Acknowledgments

The authors acknowledge the Bangladesh Railway, Bangladesh Army, and Construction Supervision Consultant (CSC) and Padma Bridge Rail Link Project (PBRLP) for providing technical support and information that facilitated this study during 2021-2022. The authors would like to give the heartiest thanks to Senior Application Engineer, Dr. Mohammed Saiful Alam Siddiquee at Bentley Systems Inc.,

USA, for his valuable comments and suggestions regarding finite element analysis of Plaxis 3D. The authors would also like to thank Brigadier General (retired) Munirul Islam, Bangladesh Army, for his extended cooperation in terms of communicating field-level information. The research leading to these results was performed as part of the employment of the lead authors.

References

[1] Final Report on Updating Railway Master Plan, *People's Republic of Bangladesh: South Asia Subregional Economic Cooperation Railway Connectivity Investment Program*, Asian Development Bank, Mandaluyong, 2017, https://www.adb.org/sites/default/files/project-documents/46452/46452-001-tacr-en.pdf.

[2] GoB, "Making Vision 2041 a Reality: Perspective Plan of Bangladesh 2021-2041," 2020, http://oldweb.lged.gov.bd/uploadeddocument/unitpublication/1/1049/vision%202021-2041.pdf.

[3] S. R. Gales, "The hardinge bridge over the lower Ganges at sara. (Including appendices and plates at back of volume)," *Minutes of the Proceedings of the Institution of Civil Engineers*, vol. 205, no. 1918, pp. 18–67, 1918.

[4] S. A. Kuehl, M. A. Allison, S. L. Goodbred, and H. E. R. M. A. N. N. Kudrass, "The ganges-brahmaputra delta," *Special Publication-SEPM*, vol. 83, p. 413, 2005.

[5] A. Shah, S. Khan, M. H. Shah, R. Khan, and I. Jan, "Environmental impact assessment (EIA) of infrastructure development projects in developing countries," *OIDA International Journal of Sustainable Development*, vol. 1, no. 4, pp. 47–54, 2010.

[6] Bangladesh marks opening of country's longest bridge, The Washington Post, 2022, https://www.washingtonpost.com/world/bangladesh-marks-opening-of-countrys-longest-bridge/2022/06/25/3ffd3b4a-f45f-11ec-ac16-8fbf7194cd78_story.html Retrieved from:.

[7] A. Jazeera, "PM Hasina Opens Bangladesh's Longest Bridge over River Padma," 2022, https://www.aljazeera.com/news/2022/6/25/bangladesh-unveils-its-longest-bridge-over-river-padma Retrieved from:.

[8] China Railway Engineering and Construction, "CREC project management office of Padma bridge rail Link project," 2021, https://www.railway-technology.com/projects/padma-bridge-rail-link-project-bangladesh/ Report No. BD/PDMBRP/DD-CS/TM/OU/2021/7162.

[9] M. Burrow, P. Teixeira, T. Dahlberg, and E. Berggren, "Track stiffness considerations for high-speed railway lines," *Railway transportation: Policies, Technology and Perspectives*, vol. 14, pp. 303–354, 2009.

[10] K. Dong, D. P. Connolly, O. Laghrouche, P. K. Woodward, and P. Alves Costa, "The stiffening of soft soils on railway lines," *Transportation Geotechnics*, vol. 17, pp. 178–191, 2018.

[11] A. J. F. Duley, L. Le Pen, D. J. Thompson et al., "Critical Train Speeds and Associated Track Movements–A Case Study," *Institution of Civil Engineers*, vol. 21, 2015.

[12] D. Y. Jeong, "Analyses for lateral deflection of railroad track under quasi- static loading," *Rail Transportation Division Conference*, vol. 56116, 2013, October.

[13] H. Jiang, X. Bian, C. Cheng, Y. Chen, and R. Chen, "Simulating train moving loads in physical model testing of railway infrastructure and its numerical calibration," *Acta Geotechnica*, vol. 11, no. 2, pp. 231–242, 2016.

[14] Y. Jiang and S. Nimbalkar, "Finite Element modeling of ballasted rail track capturing effects of geosynthetic inclusions," *Frontiers in Built Environment*, vol. 5, p. 69, 2019.

[15] B. Picoux and D. Le Houedec, "Diagnosis and prediction of vibration from railway trains," *Soil Dynamics and Earthquake Engineering*, vol. 25, no. 12, pp. 905–921, 2005.

[16] M. Shahraki, M. R. S. Sadaghiani, K. J. Witt, and T. Meier, "3D modelling of train induced moving loads on an embankment," *Plaxis Bulletin*, vol. 36, pp. 10–15, 2014.

[17] C. Tang, Z. Lu, H. Yao, S. Guo, X. Huang, and J. Liu, "Semi analytical solution for dynamic responses of railway track system on unsaturated poro-elastichalf-space subjected to moving trainload," *International Journal*, vol. 10, no. 1, 2021.

[18] J. Vinter and L. K. Tanttu, "The effect of the sub-ballast layer material to the performance of a railway embankment," in *Proceedings of the 24th European Young Geotechnical Engineers Conference*, pp. 11–13, Durham University, Beijing China, September 2015.

[19] Q. Fu and C. Zheng, "Three-dimensional dynamic analyses of track-embankment-ground system subjected to high-speed train loads," *The Scientific World Journal*, vol. 2014, Article ID 924592, 2014.

[20] A. Elgamal, "Simulate the Failure of Embankment Due to High-Speed Train Moving Load," in *Proceedings of the 5th World Congress on Civil, Structural, and Environmental Engineering*, Lisbon, Portugal, Octomber 2020.

[21] S. Krabbenhoft and R. Christensen, "Design of railway embankment using the Mohr coulomb criterion and GSK model for cohesionless soil," in *Advances in Engineering Materials, Structures and Systems: Innovations, Mechanics and Applications*, pp. 2292–2296, CRC Press, Boca Raton, Fl, 2019.

[22] S. Likitlersuang, P. Pholkainuwatra, T. Chompoorat, and S. Keawsawasvong, "Numerical modelling of railway embankments for high-speed train constructed on soft soil," *Journal of GeoEngineering*, vol. 13, no. 3, pp. 149–159, 2018.

[23] M. J. Moghadam and K. Ashtari, "Numerical analysis of railways on soft soil under various train speeds," *Transportation Infrastructure Geotechnology*, vol. 7, no. 1, pp. 103–125, 2020.

[24] J. J. Muhammed, P. W. Jayawickrama, A. Teferra, and M. A. Özer, "Settlement of a railway embankment on PVD-improved Karakore soft alluvial soil," *Engineering Science and Technology, an International Journal*, vol. 23, no. 5, pp. 1015–1027, 2020.

[25] T. Thorsen, "Load bearing capacity of railway embankments," in *Proceedings of the 17thNordic Geotechnical Meeting Challenges in Nordic Geotechnic*, Seoul Korea, May 2016.

[26] G. Lazorenko, A. Kasprzhitskii, A. Kukharskii, A. Kochur, and V. Yavna, "Failure analysis of widened railway embankment with different reinforcing measures under heavy axle loads: a comparative FEM study," *Transport Engineer*, vol. 2, Article ID 100028, 2020.

[27] *PLAXIS Materials Model Manual*, Bentley Systems, USA, 2021.

[28] L. Hall, "Simulations and analyses of train-induced ground vibrations in finite element models," *Soil Dynamics and Earthquake Engineering*, vol. 23, no. 5, pp. 403–413, 2003.

[29] E. T. Selig and A. Sluz, "Ballast and subgrade response to train loads," *Transportation Research Record*, vol. 694, 1978.

[30] B. Indraratna and S. Nimbalkar, "Stress-strain degradation response of railway ballast stabilized with geosynthetics," *Journal of Geotechnical and Geoenvironmental Engineering*, vol. 139, no. 5, pp. 684–700, 2013.

[31] R. A. P. C Costa, a Silva Cardoso, and A. Bodare, "Influence of soil non-linearity on the dynamic response of high-speed railway tracks [J]," *Soil Dynamics and Earthquake Engineering*, vol. 30, pp. 221–235, 2010.
[32] L. Fang and Z. G. Zhu, "Study of influence factors of lateral deformation of soft soil foundation under embankments," *Highway Transp Sci Technol*, vol. 11, pp. 38–42, 2005.
[33] F. Tavenas, C. Mieussens, and F. Bourges, "Lateral displacements in clay foundations under embankments," *Canadian Geotechnical Journal*, vol. 16, no. 3, pp. 532–550, 1979.
[34] J. L. Han and Y. Zhao, "Analysis on the settlement characteristics of lateral displacement of the high embankments," *J Wuhan Univ Technol Transp Sci Eng*, vol. 36, pp. 165–167, 2012.
[35] G. H. Lv, W. Cui, and S. J. Wang, "Model test and theoretical analysis of new and old embankments differential settlement considering lateral deformation," *Geotechnical and Geological Engineering*, vol. 39, no. 8, pp. 5743–5751, 2021.
[36] G. F. Pan, X. F. Liu, S. Y. Yuan, D. X. Sun, and K. Xiao, "Lateral defor-mation of embankment with the CFG pile-net structure forYun-Gui passenger dedicated line," *Rock and Soil Mechanics*, vol. 2, pp. 1–11, 2020.
[37] H. G. Poulos, C. Y. Lee, and J. C. Small, "Prediction of embankment performance on Malaysian marine clays," *Int. Symp. Trial Embankments Malaysian Mar Clays*, vol. 3, pp. 22–31, 1989.
[38] P. V. Long, D. T. Bergado, L. V. Nguyen, and A. S. Balasubramaniam, "Design and performance of soft ground improvement using PVD with and without vacuum consolidation," *Geotech. Eng. J. SEAGS AGSSEA*, vol. 44, pp. 36–51, 2013.
[39] M. Y. Fattah, M. R. Mahmood, and M. F. Aswad, "Effect of track speed on the behavior of railway track ballast system underlain by clay IOP Conference Series: materials Science and Engineering," *IOP Conference Series: Materials Science and Engineering*, vol. 737, no. 1, 012114 pages, 2020, February.
[40] A. Kalliainen, P. Kolisoja, and A. Nurmikolu, *Radan 3Drakennemalli Ja Ratarakenteen Kuormituskestävyys*, Finnish Transport Agency, Helsinki, 2014.
[41] *User's Manual for the Operation of the Microtremor Observation System*, Buttan Service Co., Ltd, Tokyo, 2010.
[42] Y. Nakamura, "A method for dynamic characteristics estimation of subsurface using microtremor on the ground surface," *Quarterly Reports*, vol. 30, no. 1, 1989.
[43] Y. Nakamura, "Seismic vulnerability indices for ground and structures using microtremor," in *World Congress on Railway Research in Florence*Italy, 1997.
[44] Sesame, *Site Effects Assessment Using Ambient Excitations: Final Report*, European Commission Research General Directorate, Project EVG1-CT-2000-00026 SESAME, China, 2004.
[45] M. Z. Rahman, A. S. M. M. Kamal, and S. Siddiqua, "Near-surface shear wave velocity estimation and V s 30 mapping for Dhaka City, Bangladesh," *Natural Hazards*, vol. 92, no. 3, pp. 1687–1715, 2018.
[46] *Easy Hvsr user manual*, GeoStru Software, NY China, 2013.
[47] H. V. P. Truong, "Added soil mass and ratio of damping for vertical and HorizontalVibration," in *Proceedings of the 11th Conference on Science and Technology*, pp. 24–30, University of Technology in Saigon, Vietnam National University, Vietnam, October 2009.
[48] H. V. P. Truong, "Dynamic soil mass and resonant frequency of pile foundations," in *Proceedings of the 14th Asian Regional Conference on Soil Mechanics and Geotechnical Engineering*, Hong Kong, May 2011.
[49] H. V. P. Truong, "Dynamic spring constants and effect of frequency on footing vibration," in *Proceedings of the 14th Asian Regional Conference on Soil Mechanics and Geotechnical Engineering*, Hong Kong, May 2011.
[50] S. Boudaa, S. Khalfallah, and E. Bilotta, "Static interaction analysis between beam and layered soil using a two-parameter elastic foundation," *International Journal of Advanced Structural Engineering*, vol. 11, no. 1, pp. 21–30, 2019.
[51] H. S. Chore, R. K. Ingle, and V. A. Sawant, "Building frame-pilefoundation-soil interaction analysis: a parametric study," *Interaction and Multiscale Mechanics*, vol. 3, no. 1, pp. 55–79, 2010.
[52] S. M. Kim and S. Yang, "Moving two-axle high frequency harmonic loads on axially loaded pavement systems," *KSCE Journal of Civil Engineering*, vol. 14, no. 4, pp. 513–526, 2010.
[53] S. Limkatanyu, M. Kwon, W. Prachasaree, and P. Chaiviriyawong, "Contact-interfacefiber-section element: shallow foundation modeling," *Geomechanics and Engineering*, vol. 4, no. 3, pp. 173–190, 2012.
[54] P. Raychowdhury, "Seismic response of low-rise steel moment-resisting frame (SMRF) buildings incorporating nonlinear soil–structure interaction (SSI)," *Engineering Structures*, vol. 33, no. 3, pp. 958–967, 2011.
[55] E. J. Sapountzakis and A. E. Kampitsis, "Nonlinear analysis of shear deformable beam-columns partially supported on tensionless three-parameter foundation," *Archive of Applied Mechanics*, vol. 81, no. 12, pp. 1833–1851, 2011.
[56] M. Shahraki, "Numerical Analysis of Soil Behavior and Stone Columns Effects on the Railway Track (Doctoral Dissertation, Bauhaus-Universität Weimar)," 2019, https://e-pub.uni-weimar.de/opus4/frontdoor/deliver/index/docId/4015/file/Shahraki_Numerical_Analysis.pdf.
[57] B. Sathishkumar, K. M. Mohanasundaram, and M. S. Kumar, "Impact of particle damping parameters on surface roughness of bored surface," *Arabian Journal for Science and Engineering*, vol. 39, no. 10, pp. 7327–7334, 2014.
[58] G. C. Beroza, H. Kanamori, Y. Fialko et al., "Treatise on geophysics," *Earthquake Seismology*, vol. 10, pp. 1–58, 2007.
[59] A. Kalliainen and P. Kolisoja, *Ratapenkereiden Leveys Ja Luiskakaltevuus*, Väliraportti. Finnis Transport Agency, Helsinki, 2009.
[60] H. Wang, L. L. Zeng, X. Bian, and Z. S. Hong, "Train moving load-induced vertical superimposed stress at ballasted railway tracks," *Advances in Civil Engineering*, vol. 2020, Article ID 3428395, 2020.
[61] P. Punetha, K. Maharjan, and S. Nimbalkar, "Finite element modeling of the dynamic response of critical zones in a ballasted railway track," *Frontiers in Built Environment*, vol. 7, p. 42, 2021.
[62] M. S. Abebe and H. S. Qiu, "Numerical modeling of geotextile reinforcement of soft subgrade ballasted railway under high-speed train," *Electronic Journal of Geotechnical Engineering EJGE*, vol. 21, pp. 4227–4343, 2016.
[63] M. Y. Fattah, M. R. Mahmood, and M. F. Aswad, "Stress distribution from railway track over geogrid reinforced ballast underlain by clay," *Earthquake Engineering and Engineering Vibration*, vol. 18, no. 1, pp. 77–93, 2019.
[64] M. Y. Fattah, M. R. Mahmood, and M. F. Aswad, "Stress waves transmission from railway track over geogrid reinforced ballast underlain by clay," *Structural Monitoring and Maintenance*, vol. 9, no. 1, pp. 1–27, 2022.

[65] J. Hu, X. Bian, and J. Jiang, "Critical velocity of high-speed train running on soft soil and induced dynamic soil response," *Procedia Engineering*, vol. 143, pp. 1034–1042, 2016.
[66] S. S. Jeon, "Settlement and bearing capacity of roadbed subjected to tilting-train loading in various ground conditions," *International Journal of Railway*, vol. 8, no. 2, pp. 35–41, 2015.
[67] S. Aziz, J. R. Mallick, I. L. Hoque, M. A. Nayeem, and A. F. M. S. Amin, "Behavior of railway embankment constructed on soft deltaic deposits under varying train speed," in *Proceedings of the International Conference on Civil Engineering and Material Science*, Chiba, Japan, June 2022.
[68] M. Atalan, L.J. Prendergast, A. Grizi, and N Thom, "A review of numerical models for Slab-Asphalt track railways," *Infrastructures*, vol. 7, no. 4, p. 59, 2022.